Molecular Orientation Analysis of Alkyl Methylene Groups from Quantitative Coherent Anti-Stokes Raman Scattering Spectroscopy

(Supporting Information)

Chi Zhang[1], Jie Wang[1,†], Joshua Jasensky[2], Zhan Chen[1]*

1. University of Michigan, Department of Chemistry, 930 N. University Ave. Ann Arbor, MI, 48109, USA.

2. University of Michigan, Biophysics, 930 N. University Ave. Ann Arbor, MI, 48109, USA.

AUTHOR INFORMATION

Corresponding Author

* zhangchi@umich.edu, Tel: 734-389-5895

I. Experimental setup and sample preparation

The CARS experiment in this work was performed on a modified commercial SFG system (EKSPLA) with ~20 ps pulse width and 20 Hz repetition rate.[S1] The pulse energies for pump (532 nm) and Stokes (626-637 nm) beams were ~200 and ~100 μJ at sample, respectively. The experimental geometry used for CARS spectral collection is shown in Figure 1a, which is similar to our SFG geometry.[S1] Laser frequency of the Stokes beam was tuned continuously at 5 cm^{-1} per step for the generation of a CARS spectrum. Each data point on a spectrum was integrated for 2.5 s and the finial spectrum analyzed in this study was an average from five repeatedly collected spectra. The CARS signal was collected using a gated photomultiplier tube (PMT) installed on a monochromator.

Silica windows used as solid supports for the samples were obtained from Altos Photonics Inc. They were cleaned in concentrated sulfuric acid saturated with potassium dichromate overnight at 60 ºC and rinsed using deionized water. Dipalmitoyl-phosphatidylglycerol (DPPG) lipid powder was purchased from Avanti Polar lipid and used as arrived. DPPG lipid monolayer was deposited on a silica window using Langmuir Bloddget method.[S2] Octadecyltrimethoxysilane (OTMS) was purchased from Sigma Aldrich and was grown on silica windows using procedures mentioned in section X.

II. Fresnel factors

The third order effective nonlinear susceptibility obtained from a CARS spectrum can be further correlated to the local third order nonlinear susceptibility of the material through the following equation:

$$\chi^{(3)}_{eff,ABCD} = \sum_{IJKL=x,y,z} M \cdot L_{AI}(\omega_{CARS}) L_{BJ}(\omega_p) L_{CK}(\omega_p) L_{DL}(\omega_s) \cdot \chi^{(3)}_{IJKL}, \quad A,B,C,D = s,p \quad \text{(S1)}$$

Here $\chi^{(3)}_{IJKL}$ is a local nonlinear susceptibility element of the sample in the lab frame (defined by *x, y, z*). The indices *I, J, K, L* represent coordinates in the lab-fixed frame system, and *A, B, C, D* indices represent polarization combinations (*s* or *p*) of the CARS experiment (*A*-polarized CARS signal beam, *B*-polarized pump beam, *C*-polarized probe beam, *D*-polarized Stokes beam). M is a factor multiplying all the trigonometric factors of the projected input electric field on the lab frame coordinate axis.

The detailed L factors are [S3]

$$L_{sy} = \frac{2n_1(\omega)\cos\beta}{n_1(\omega)\cos\beta + n_2(\omega)\cos\gamma},$$
$$L_{px} = \frac{2n_1(\omega)\cos\gamma}{n_1(\omega)\cos\gamma + n_2(\omega)\cos\beta}, \quad \text{(S2)}$$
$$L_{pz} = \frac{2n_2(\omega)\cos\beta}{n_1(\omega)\cos\gamma + n_2(\omega)\cos\beta}\left(\frac{n_1(\omega)}{n'(\omega)}\right),$$

$n_1(\omega)$ is the refractive index of air, which equals to 1.00; the silica window refractive index $n_2(\omega) = 1.45$; the lipid refractive index $n'(\omega)$ was taken as 1.45. The angle β is the input angle of the laser beam while γ is the refractive angle in the silica window. ω is the input laser frequency. The input angles of the pump/probe and Stokes beams used in the experiment were ~60° and 55°, respectively. The 532 nm laser beam was used as the pump/probe beam; the Stokes beam wavelength for the 2880 cm^{-1} Raman transition was 628 nm; the corresponding CARS signal was generated at 461 nm.

For measurements in *ssss* and *spps* polarization combinations:

$$\chi^{(3)}_{eff,ssss} = 1 \cdot L_{sy}(\omega_{CARS})L_{sy}(\omega_p)L_{sy}(\omega_p)L_{sy}(\omega_s) \cdot \chi^{(3)}_{yyyy} \quad \text{(S3)}$$

$$\chi^{(3)}_{eff,spps} = \cos^2\theta_p \cdot L_{sy}(\omega_{CARS})L_{px}(\omega_p)L_{px}(\omega_p)L_{sy}(\omega_s) \cdot \chi^{(3)}_{yxxy} + \sin^2\theta_p \cdot L_{sy}(\omega_{CARS})L_{pz}(\omega_p)L_{pz}(\omega_p)L_{sy}(\omega_s) \cdot \chi^{(3)}_{yzzy} \quad \text{(S4)}$$

Plugging in the numbers we can obtain:

$$\left|\frac{\chi^{(3)}_{ssss}}{\chi^{(3)}_{spps}}\right| \approx \left|\frac{0.13\chi^{(3)}_{yyyy}}{0.099\chi^{(3)}_{yxxy} + 0.054\chi^{(3)}_{yzzy}}\right| \quad \text{(S5)}$$

For an isotropic bulk material $\chi^{(3)}_{yxxy} = \chi^{(3)}_{yzzy}$, then $\left|\frac{\chi^{(3)}_{ssss}}{\chi^{(3)}_{spps}}\right| \approx 0.85\left|\frac{\chi^{(3)}_{yyyy}}{\chi^{(3)}_{yxxy}}\right|$. However, for materials without inversion symmetry, $\chi^{(3)}_{yxxy}$ and $\chi^{(3)}_{yzzy}$ may not equal. Therefore, for the non-centrosymmetric case, only eq (S5) is satisfied.

III. Transformation matrix R

Euler angle system is usually used for the structural analysis in the molecular frame, which involves three angles: azimuthal angle ϕ, tilt angle θ and twist angle ψ, as defined in Figure 1c in the paper. In Euler angle system, the projection of molecules from one coordinate system to the other requires rotation operations, which are mathematically performed using transformation matrices. The transformation matrices of rotations (counter-clockwise) with respect to *x, y, z* or *a, b, c* axes for α degree are:

$$\mathbf{R}_{x(\text{or } a)} = \begin{bmatrix} 1 & 0 & 0 \\ 0 & \cos\alpha & \sin\alpha \\ 0 & -\sin\alpha & \cos\alpha \end{bmatrix},$$
$$\mathbf{R}_{y(\text{or } b)} = \begin{bmatrix} \cos\alpha & 0 & -\sin\alpha \\ 0 & 1 & 0 \\ \sin\alpha & 0 & \cos\alpha \end{bmatrix}, \quad \text{(S6)}$$
$$\mathbf{R}_{z(\text{or } c)} = \begin{bmatrix} \cos\alpha & \sin\alpha & 0 \\ -\sin\alpha & \cos\alpha & 0 \\ 0 & 0 & 1 \end{bmatrix}$$

To overlap two coordinate systems, usually three rotations combinations are needed. In this work we chose *z-y-z* rotation combination, which gives:

$$\mathbf{R}_{z-y-z} = \begin{bmatrix} \cos\psi & \sin\psi & 0 \\ -\sin\psi & \cos\psi & 0 \\ 0 & 0 & 1 \end{bmatrix} \begin{bmatrix} \cos\theta & 0 & -\sin\theta \\ 0 & 1 & 0 \\ \sin\theta & 0 & \cos\theta \end{bmatrix} \begin{bmatrix} \cos\phi & \sin\phi & 0 \\ -\sin\phi & \cos\phi & 0 \\ 0 & 0 & 1 \end{bmatrix}$$
$$= \begin{bmatrix} \cos\phi\cos\theta\cos\psi - \sin\phi\sin\psi & \cos\theta\cos\psi\sin\phi + \cos\phi\sin\psi & -\cos\psi\sin\theta \\ -\cos\psi\sin\phi - \cos\phi\cos\theta\sin\psi & \cos\phi\cos\psi - \cos\theta\sin\phi\sin\psi & \sin\theta\sin\psi \\ \cos\phi\sin\theta & \sin\phi\sin\theta & \cos\theta \end{bmatrix} \quad \text{(S7)}$$

This transformation matrix is used for the angle averaging in eq (2) and (3) in the paper. The angle averaging is taken from 0 to 2π for ϕ and ψ, and from 0 to π for θ.

Here we define:

$$\mathbf{R}_x = \begin{bmatrix} \cos\phi\cos\theta\cos\psi - \sin\phi\sin\psi & \cos\theta\cos\psi\sin\phi + \cos\phi\sin\psi & -\cos\psi\sin\theta \end{bmatrix}$$

$$\mathbf{R}_y = \begin{bmatrix} -\cos\psi\sin\phi - \cos\phi\cos\theta\sin\psi & \cos\phi\cos\psi - \cos\theta\sin\phi\sin\psi & \sin\theta\sin\psi \end{bmatrix}$$

$$\mathbf{R}_z = \begin{bmatrix} \cos\phi\sin\theta & \sin\phi\sin\theta & \cos\theta \end{bmatrix}$$

$\mathbf{R}_x^T$, $\mathbf{R}_y^T$ and $\mathbf{R}_z^T$ are the corresponding transposes of the matrices.

IV. Calculation of third order nonlinear susceptibility components

Third order nonlinear susceptibility can be calculated as:

$$\boldsymbol{\chi}^{(3)} = \frac{N}{4\pi^3}\int_0^{\pi}\int_0^{2\pi}\int_0^{2\pi} \mathbf{R}\otimes\mathbf{R}\otimes\mathbf{R}\otimes\mathbf{R}\cdot\boldsymbol{\gamma}^{(3)}\sin\theta\,\mathrm{d}\phi\,\mathrm{d}\psi\,\mathrm{d}\theta \qquad \text{(S8)}$$

Here $\boldsymbol{\chi}^{(3)}$ and $\boldsymbol{\gamma}^{(3)}$ are matrices of 81 elements. $\mathbf{R}$ is the 3 by 3 rotation transformation matrix as mentioned above (eq S7). The sign $\otimes$ indicates kronecker product. Dimensional analysis using eq (S8) can simultaneously calculate all the 81 components but requires a large amount of computation. Since only a few of the elements are measured in our experiment (only $\chi^{(3)}_{yyyy}$, $\chi^{(3)}_{yxxy}$ and $\chi^{(3)}_{yzzy}$), we used a method to calculate selected components individually by rotating the reference frame on the individual $\boldsymbol{\alpha}$ matrix, as discussed below. These two methods are identical in obtaining the susceptibility component $\chi^{(3)}_{IJKL}$.

As mentioned in the main text, the frequency degeneracy of the pump and probe beams in CARS gives rise to the measurement of both $\gamma^{(3)}_{ijkl}$ and $\gamma^{(3)}_{ikjl}$ contributions. Using eq (S8), it is easy to prove that for $\chi^{(3)}_{yyyy}$, $\chi^{(3)}_{yxxy}$ and $\chi^{(3)}_{yzzy}$ which will be measured in this paper, the contributions from $\gamma^{(3)}_{ijkl}$ and $\gamma^{(3)}_{ikjl}$ are equal. One easy way to think about this equality is the exchange of indices *j* and *k* in $\gamma^{(3)}_{ijkl}$ for matrix $\boldsymbol{\gamma}^{(3)}$ equals the exchange of indices *J* and *K* in $\chi^{(3)}_{IJKL}$ for matrix $\boldsymbol{\chi}^{(3)}$. However, since the *J* and *K* indices

are identical in components $\chi^{(3)}_{yyyy}$, $\chi^{(3)}_{yxxy}$ and $\chi^{(3)}_{yzzy}$, the exchange of *J* and *K* does not affect these components. Therefore, we can simply use eq (3) in the main text to calculate $\chi^{(3)}_{IJKL}$.

To obtain each individual susceptibility component $\chi^{(3)}_{IJKL}$, we can rotate the reference frame on the individual $\boldsymbol{\alpha}$ matrix, For example:

$$\chi^{(3)}_{yyyy} = \frac{C \cdot N}{4\pi^3} \int_0^{\pi} \int_0^{2\pi} \int_0^{2\pi} \mathbf{R}_y \boldsymbol{\alpha}' \mathbf{R}_y^T \mathbf{R}_y \boldsymbol{\alpha}' \mathbf{R}_y^T \sin\theta \mathrm{d}\phi \mathrm{d}\psi \mathrm{d}\theta \tag{S9}$$

$$\chi^{(3)}_{yxxy} = \frac{C \cdot N}{4\pi^3} \int_0^{\pi} \int_0^{2\pi} \int_0^{2\pi} \mathbf{R}_y \boldsymbol{\alpha}' \mathbf{R}_x^T \mathbf{R}_x \boldsymbol{\alpha}' \mathbf{R}_y^T \sin\theta \mathrm{d}\phi \mathrm{d}\psi \mathrm{d}\theta \tag{S10}$$

V. Bond additivity calculation for Raman tensor derivatives of methylene group and methylene alkyl chain

A single C-H bond possesses $C_{\infty v}$ symmetry, therefore its Raman tensor derivative can be expressed as:

$$\boldsymbol{\alpha}'_{C-H} = \alpha'_{cc} \begin{bmatrix} r & 0 & 0 \\ 0 & r & 0 \\ 0 & 0 & 1 \end{bmatrix} \tag{S11}$$

To overlap (*a', b', c'*) and (*a'', b'', c''*) with (*a, b, c*) coordinates respectively using the coordinate system defined in Figure 1c and the transformation matrices, we have for CH bond 1 and bond 2:

$$\boldsymbol{\alpha}'_{C-H1} = R_{c':-54.5} R_{b':-90} \boldsymbol{\alpha}'_{C-H} R^T_{b':-90} R_{c':-54.5}$$

$$\boldsymbol{\alpha}'_{C-H2} = R_{c':54.5} R_{b':-90} \boldsymbol{\alpha}'_{C-H} R^T_{b':-90} R_{c':54.5}$$

Here CH bond 1 is firstly rotated -90° with respect to the *b'* axis, then is rotated -54.5° with respect to the *c'* axis. The CH bond 2 is firstly rotated -90° with respect to the *b''* axis, then is rotated 54.5° with respect to the *c''* axis.

Methylene group vibrational stretching modes can be expressed in the normal mode coordinates:[S4]

$$Q_s = (\Delta r_1 + \Delta r_2)/(2G_s)^{1/2}$$
$$Q_{as} = (\Delta r_1 - \Delta r_2)/(2G_{as})^{1/2} \quad \text{(S12)}$$

Here Δr_n is the bond displacement vector along the direction of the nth C-H bond. G_s and G_{as} are inverted reduced masses of the symmetric and asymmetric modes:

$$G_s = \frac{1+\cos\tau}{M_C} + \frac{1}{M_H}$$
$$G_{as} = \frac{1-\cos\tau}{M_C} + \frac{1}{M_H} \quad \text{(S13)}$$

The angle τ is the H-C-H bond angle which is 109.5°. M_C and M_H are atomic masses of the carbon and hydrogen atoms. We can then calculate $G_s = 1.06$ and $G_{as} = 1.11$.

Accordingly, for the CH_2 symmetric and asymmetric modes:

$$\boldsymbol{\alpha}'_{C-H,s} = (R_{c':-54.5}R_{b':-90}\boldsymbol{\alpha}'_{C-H}R^T_{b':-90}R_{c':-54.5} + R_{c':54.5}R_{b':-90}\boldsymbol{\alpha}'_{C-H}R^T_{b':-90}R_{c':54.5})/\sqrt{2\times 1.06}$$

$$\boldsymbol{\alpha}'_{C-H,as} = (R_{c':-54.5}R_{b':-90}\boldsymbol{\alpha}'_{C-H}R^T_{b':-90}R_{c':-54.5} - R_{c':54.5}R_{b':-90}\boldsymbol{\alpha}'_{C-H}R^T_{b':-90}R_{c':54.5})/\sqrt{2\times 1.11}$$

Considering the energy coupling between methylene group with bonds outside the group, and the possible energy coupling between different vibrational modes, here we apply a factor *b* to modify the energy ratio between the symmetric mode and thus:[S4]

$$\boldsymbol{\alpha}'_{C-H,s} = b\times(R_{c':-54.5}R_{b':-90}\boldsymbol{\alpha}'_{C-H}R^T_{b':-90}R_{c':-54.5} + R_{c':54.5}R_{b':-90}\boldsymbol{\alpha}'_{C-H}R^T_{b':-90}R_{c':54.5})/\sqrt{2\times 1.06}$$

The value of *b* could be derived from CARS experimental data of bulk materials, as discussed in the paper.

Using eq (S6) and (S11), we have:

$$\boldsymbol{\alpha}'_s = b\times\alpha'_{cc}\begin{bmatrix} 0.477+0.937r & 0 & 0 \\ 0 & 0.937+0.477r & 0 \\ 0 & 0 & 1.414r \end{bmatrix} \quad \text{(S14)}$$

$$\boldsymbol{\alpha}'_{as} = \alpha'_{cc}\begin{bmatrix} 0 & -0.669+0.669r & 0 \\ -0.669+0.669r & 0 & 0 \\ 0 & 0 & 0 \end{bmatrix} \quad \text{(S15)}$$

For a lipid methylene alkyl chain adopting a trans-arrangement, similar conclusion could be derived. The combination of the two adjacent CH_2 groups requires an additional 180º rotation on one group with respect to the *c* axis. According to eq (S6), this transformation matrix is a unit matrix. Therefore, the Raman tensor derivatives of the alkyl chain with trans-arrangement are simply those shown in eq (S14) and (S15) multiplied by the number of CH_2 groups in the chain. In this research we simply adopted eq (S14) and (S15) to calculate the entire alkyl chain, and ignored the constant raised from the number of CH_2 groups, because such constant merged in constant C in eq (S9) and (S10) during calculation.

VI. CARS spectral fitting

CARS spectra of dipalmitoyl-phosphatidylglycerol (DPPG) lipid powder collected in *ssss* and *spps* polarizations are shown in Figure S1 and Figure 2a, respectively. The peaks at ~2855 cm^{-1} and ~2883 cm^{-1} are from the methylene symmetric and asymmetric stretching. We performed spectral fitting using eq (1) for both cases. The fitting parameters used for such fittings are listed in Table S1 and S2, respectively. The CARS spectrum of a DPPG monolayer deposited on a silica window collected in *spps* polarization is shown in Figure 2b and the corresponding spectral fitting parameters are listed in Table S2.

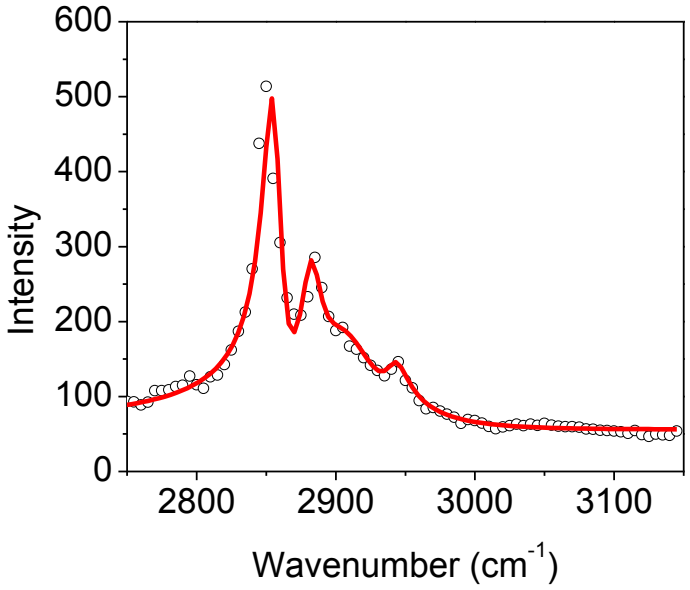

Figure S1. CARS spectrum of DPPG lipid powder collected in *ssss* polarization combination. Dots are experimental data, the line is spectral fitting result.

Table S1. CARS spectral fitting results of Figure S1.

Lipid powder		Value
Offset (*ssss*)		59.23 a.u.
$\chi^{(3)}_{NR}$ (*ssss*)		-2.00 a.u.
CH_2 symmetric mode (*ssss*)	$\mathbf{A}_s$	125.85 a.u.
	ω_s	2856 cm^{-1}
	$\mathbf{\Gamma}_s$	8.00 cm^{-1}
CH_2 asymmetric mode (*ssss*)	$\mathbf{A}_{as}$	75.12 a.u.
	ω_{as}	2884 cm^{-1}
	$\mathbf{\Gamma}_{as}$	9.13 cm^{-1}
Unassigned (*ssss*)	$\mathbf{A}$	226.23 a.u.
	ω	2895 cm^{-1}
	$\mathbf{\Gamma}$	23.85 cm^{-1}
CH_3 Fermi-resonance (*ssss*)	$\mathbf{A}_F$	48.46 a.u.
	ω_F	2942 cm^{-1}
	$\mathbf{\Gamma}_F$	10.00 cm^{-1}

Table S2. CARS spectral fitting results of Figure 2a and 2b.

	Lipid powder		Value
(Figure 2a)	Offset (*spps*)		8.01 a.u.
	$\chi^{(3)}_{NR}$ (*spps*)		0.02 a.u.
	CH_2 symmetric mode (*spps*)	$\mathbf{A}_s$	19.18 a.u.
		ω_s	2855 cm^{-1}
		$\mathbf{\Gamma}_s$	8.00 cm^{-1}
	CH_2 asymmetric mode (*spps*)	$\mathbf{A}_{as}$	67.03 a.u.
		ω_{as}	2883 cm^{-1}
		$\mathbf{\Gamma}_{as}$	9.13 cm^{-1}
	Lipid monolayer		Value
(Figure 2b)	Offset (*spps*)		3.98 a.u.
	$\chi^{(3)}_{NR}$ (*spps*)		0.10 a.u.
	CH_2 symmetric mode (*spps*)	$\mathbf{A}_s$	0.90 a.u.
		ω_s	2856 cm^{-1}
		$\mathbf{\Gamma}_s$	8.00 cm^{-1}
	CH_2 asymmetric mode (*spps*)	$\mathbf{A}_{as}$	12.40 a.u.
		ω_{as}	2883 cm^{-1}
		$\mathbf{\Gamma}_{as}$	9.13 cm^{-1}

VII. Calculation results of third order nonlinear susceptibility components

As mentioned in the paper, for an isotropic sample (molecules adopting random orientations, thus the material has inversion symmetry), all three angles ϕ, θ and ψ need to be averaged:

$$\chi^{(3)}_{IJKL} = \frac{C \cdot N}{4\pi^3} \int_0^{\pi} \int_0^{2\pi} \int_0^{2\pi} \mathbf{R}_I \boldsymbol{\alpha}' \mathbf{R}_J^T \mathbf{R}_K \boldsymbol{\alpha}' \mathbf{R}_L^T \sin\theta \, \mathrm{d}\phi \, \mathrm{d}\psi \, \mathrm{d}\theta \qquad IJKL = x, y, z \tag{S16}$$

We can plot $\left|\chi^{(3)}_{yyyy,s} / \chi^{(3)}_{yyyy,as}\right|$, $\left|\chi^{(3)}_{yxxy,s} / \chi^{(3)}_{yxxy,as}\right|$, $\left|\chi^{(3)}_{ssss,s} / \chi^{(3)}_{spps,s}\right|$ and $\left|\chi^{(3)}_{ssss,as} / \chi^{(3)}_{spps,as}\right|$ as functions of *r* as shown in Figures S2-S5.

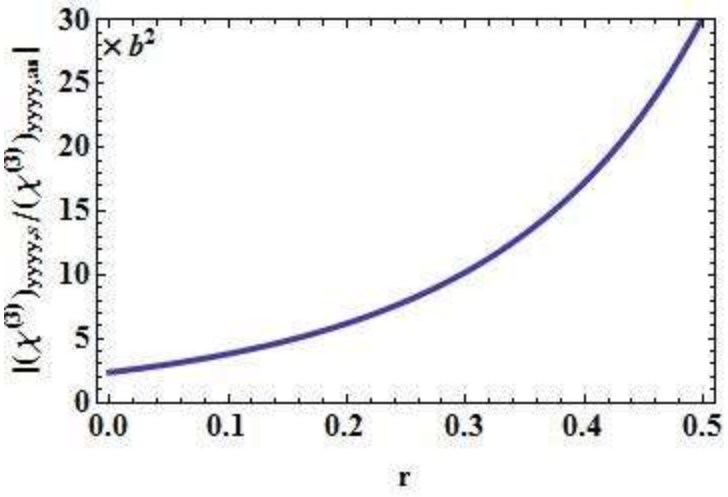

Figure S2. The value of $\left|\chi^{(3)}_{yyyy,s} / \chi^{(3)}_{yyyy,as}\right|$ as a function of *r*.

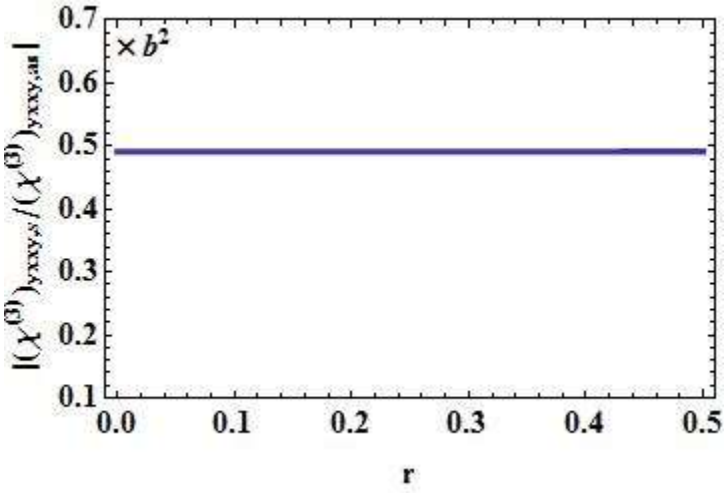

Figure S3. The value of $\left|\chi^{(3)}_{yxxy,s} / \chi^{(3)}_{yxxy,as}\right|$ as a function of *r*. The curve for $\left|\chi^{(3)}_{yzzy,s} / \chi^{(3)}_{yzzy,as}\right|$ is identical because $\chi^{(3)}_{yzzy} = \chi^{(3)}_{yxxy}$ for an isotropic sample.

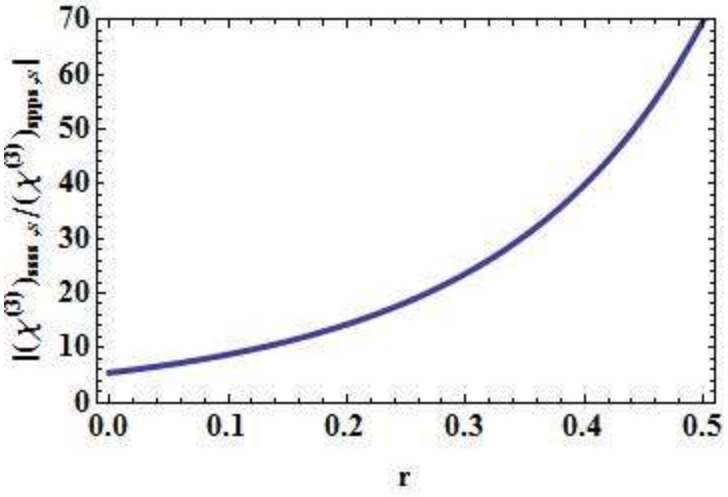

Figure S4. The value of $\left|\chi^{(3)}_{ssss,s} / \chi^{(3)}_{spps,s}\right|$ as a function of *r*. This curve is plotted based on the calculated $\left|\chi^{(3)}_{yyyy,s} / \chi^{(3)}_{yxxy,s}\right|$ curve and considering Fresnel factors $\left|\frac{\chi^{(3)}_{ssss}}{\chi^{(3)}_{spps}}\right| \approx 0.85\left|\frac{\chi^{(3)}_{yyyy}}{\chi^{(3)}_{yxxy}}\right|$.

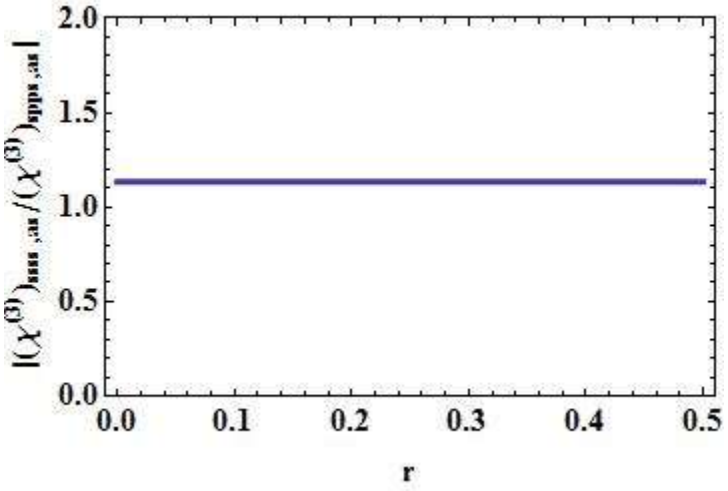

Figure S5. The value of $\left|\chi^{(3)}_{ssss,as} / \chi^{(3)}_{spps,as}\right|$ as a function of *r*. This curve is plotted based on the calculated $\left|\chi^{(3)}_{yyyy,as} / \chi^{(3)}_{yxxy,as}\right|$ curve and considering Fresnel factors $\left|\frac{\chi^{(3)}_{ssss}}{\chi^{(3)}_{spps}}\right| \approx 0.85\left|\frac{\chi^{(3)}_{yyyy}}{\chi^{(3)}_{yxxy}}\right|$.

The above figures show that when averaging all ϕ, θ and ψ angles, *r* affects the value of $\left|\chi^{(3)}_{yyyy,s} / \chi^{(3)}_{yyyy,as}\right|$. However, the values of $\left|\chi^{(3)}_{yxxy,s} / \chi^{(3)}_{yxxy,s}\right|$ and $\left|\chi^{(3)}_{yzzy,s} / \chi^{(3)}_{yzzy,s}\right|$ do not depend on *r*.

The value of *r* in eq (S11), (S14) and (S15) can be derived from Raman depolarization ratio measurement.[S5-6] This method is an empirical way and its accuracy is determined solely by the accuracy

and reliability of the Raman depolarization measurement. However, sometimes peak overlapping in Raman spectra may lead to uncertainty for the quantitative peak fitting and peak strength determination, affecting the accurate derivation of *r* value. Using the bond additivity method, CARS spectral measurement can also help to obtain the *r* value. This has been tested using PDMS methyl group CARS signal analysis, which shows that from both Raman depolarization ratio measurement and CARS peak ratio measurement, *r* could be determined to be ~0.2 for PDMS methyl group C-H bond.[S6]

In this work, we can estimate the value of *r* using CARS experimental results and our calculation. Using our method we can derive $\left|\chi^{(3)}_{spps,s} / \chi^{(3)}_{spps,as}\right| \approx 0.49b^2$. From Table S2 we have $\left|\chi^{(3)}_{spps,s} / \chi^{(3)}_{spps,as}\right| \approx 0.33$. This gives $b^2 \approx 0.67$. From the spectral fitting shown in Figure S1 and Table S1, we have $\left|\chi^{(3)}_{ssss,s} / \chi^{(3)}_{ssss,as}\right| = \left|\chi^{(3)}_{yyyy,s} / \chi^{(3)}_{yyyy,as}\right| \approx 1.9$. In Figure S2, this value corresponds to $r \approx 0.02$. This value could also be obtained from $\left|\chi^{(3)}_{ssss,s} / \chi^{(3)}_{spps,s}\right| \approx 6.5$ (Table S1 and S2), which corresponds to $r \approx 0.02$ in Figure S4. As we mentioned, *r* value affects certain nonlinear susceptibility component values but not the values of $\left|\chi^{(3)}_{yxxy,s} / \chi^{(3)}_{yxxy,as}\right|$ or $\left|\chi^{(3)}_{yzzy,s} / \chi^{(3)}_{yzzy,as}\right|$ used for spectral intensity ratio analysis and molecular orientation determination in the *spps* polarization. Therefore, the spectral fitting error in Figure S1 and the inaccuracy in *r* value will not affect our tilt angle calculation in the paper. In Figures S2 to S5, we plot the susceptibility ratio values in the range $0 \le r \le 0.5$.

From Figure S5, theoretically $\left|\chi^{(3)}_{ssss,as} / \chi^{(3)}_{spps,as}\right| \approx 1.1$. From the spectral fitting results in Table S1 and S2, we can obtain $\left|\chi^{(3)}_{ssss,as} / \chi^{(3)}_{spps,as}\right| \approx 1.1$. This indicates our Fresnel factor determination is valid.

For molecular tilt angle orientation analysis of surface functional groups, we only average ϕ and ψ using the following equation (assuming free twist rotation):

$$\chi^{(3)}_{IJKL}(\theta) = \frac{C \cdot N}{4\pi^2} \int_0^{2\pi} \int_0^{2\pi} \mathbf{R}_I \boldsymbol{\alpha}' \mathbf{R}_J^T \mathbf{R}_K \boldsymbol{\alpha}' \mathbf{R}_L^T \mathrm{d}\phi \mathrm{d}\psi \qquad IJKL = x, y, z \tag{S17}$$

In the following figures we plot the calculated susceptibility ratios as functions of the tilt angle θ, using both r=0 and r=0.5.

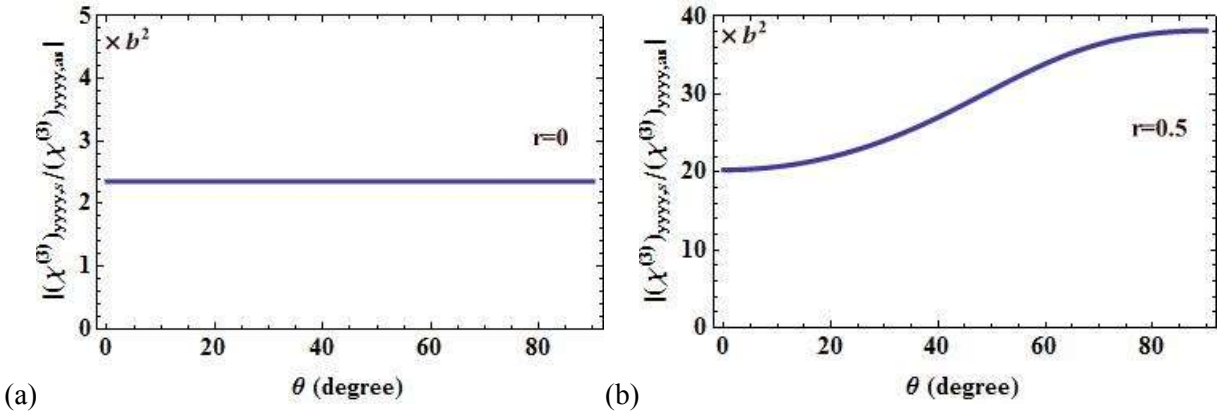

Figure S6. (a) The value of $\left|\chi^{(3)}_{yyyy,s} / \chi^{(3)}_{yyyy,as}\right|$ as a function of tilt angle θ when r=0 and (b) r=0.5.

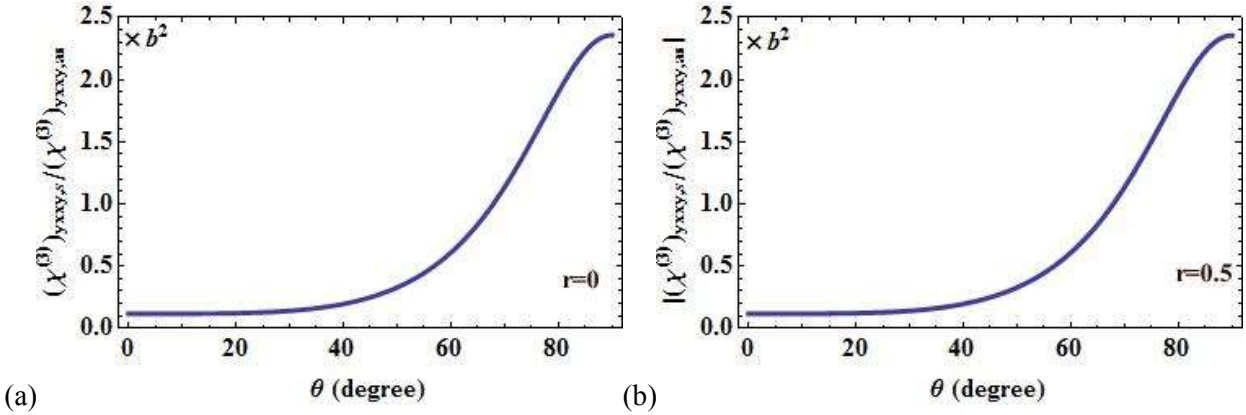

Figure S7. (a) The value of $\left|\chi^{(3)}_{yxxy,s} / \chi^{(3)}_{yxxy,as}\right|$ as a function of tilt angle θ when r=0 and (b) r=0.5.

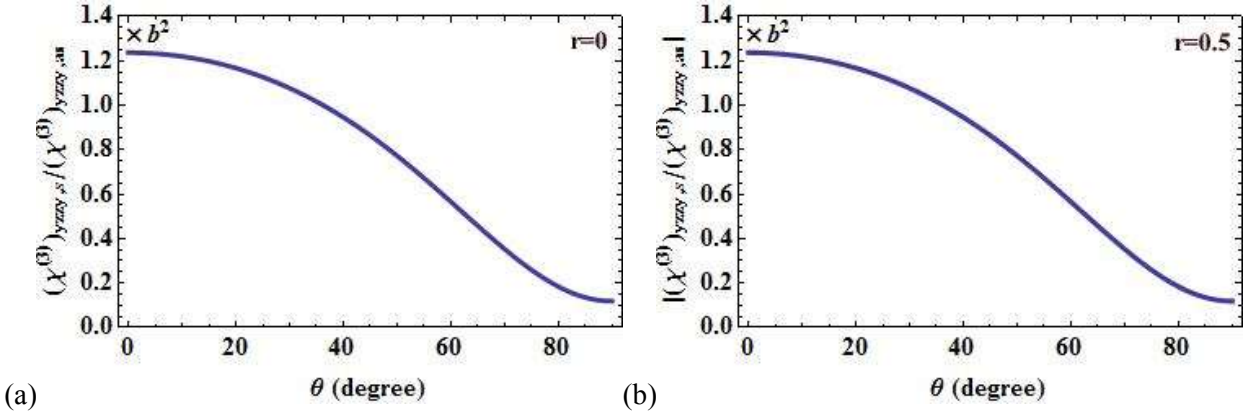

Figure S8. (a) The value of $\left|\chi^{(3)}_{yzzy,s} / \chi^{(3)}_{yzzy,as}\right|$ as a function of tilt angle θ when r=0 and (b) r=0.5.

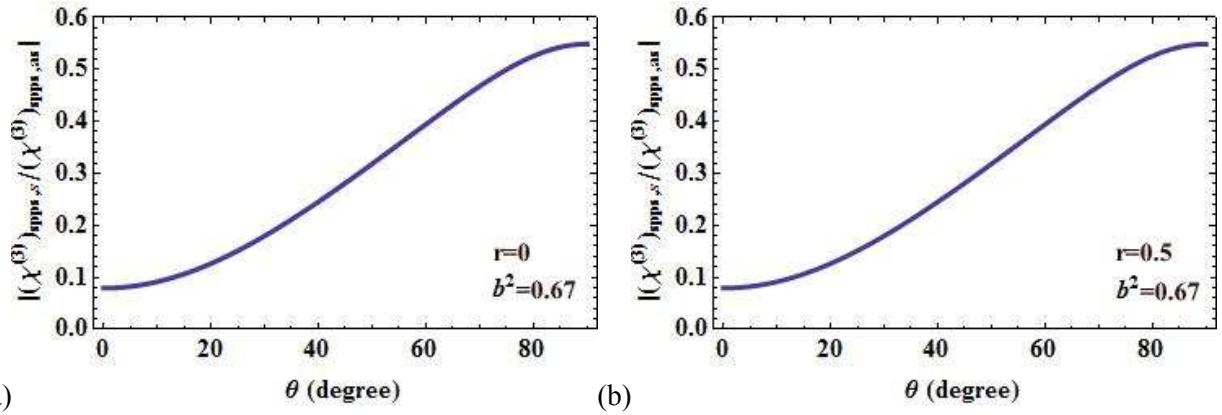

Figure S9. (a) The value of $\left|\chi^{(3)}_{spps,s} / \chi^{(3)}_{spps,as}\right|$ as a function of tilt angle θ when r=0 and (b) r=0.5. For both figures $b^2 = 0.67$.

From these figures we find that the value of $\left|\chi^{(3)}_{yyyy,s} / \chi^{(3)}_{yyyy,as}\right|$ is r dependent. However, the values of $\left|\chi^{(3)}_{yxxy,s} / \chi^{(3)}_{yxxy,as}\right|$, $\left|\chi^{(3)}_{yzzy,s} / \chi^{(3)}_{yzzy,as}\right|$ and $\left|\chi^{(3)}_{spps} / \chi^{(3)}_{spps}\right|$ are r independent. For Figure S9,

$$\begin{aligned}\left|\chi^{(3)}_{spps,s} / \chi^{(3)}_{spps,as}\right| &= b^2 \times \left|\left(0.099\chi^{(3)}_{yxxy,s} + 0.054\chi^{(3)}_{yzzy,s}\right) / \left(0.099\chi^{(3)}_{yxxy,as} + 0.054\chi^{(3)}_{yzzy,as}\right)\right| \\ &= 0.67 \times \left|\left(0.099\chi^{(3)}_{yxxy,s} + 0.054\chi^{(3)}_{yzzy,s}\right) / \left(0.099\chi^{(3)}_{yxxy,as} + 0.054\chi^{(3)}_{yzzy,as}\right)\right|\end{aligned} \quad \text{(S18)}$$

has different values when θ is different. Using this curve, we can derive molecular tilt angle of methylene groups in DPPG monolayer. The curve shown in Figure S9 is plotted in the main text as Figure 2c.

VIII. Fitting results of the SFG spectra

The spectral fitting results using the following equation[S7]

$$\left|\chi^{(2)}_{eff}\right| = \left|\chi^{(2)}_{NR} + \sum_q \frac{A_q}{\omega_{IR} - \omega_q + i\Gamma_q}\right| \quad \text{(S19)}$$

for the SFG spectra collected in the experiment are listed in Table S3.

Table S3. SFG spectral fitting results of Figure 3a and 3b.

			Value
(Figure 3a)	Offset (*ssp*)		5.69 a.u.
	$\chi_{NR}^{(3)}$ (*ssp*)		0.94 a.u.
	Symmetric mode (*ssp*)	$\mathbf{A}_s$	88.09 a.u.
		ω_s	2880 cm^{-1}
		$\mathbf{\Gamma}_s$	7.38 cm^{-1}
	Fermi resonance (*ssp*)	$\mathbf{A}_F$	97.48 a.u.
		ω_F	2942 cm^{-1}
		$\mathbf{\Gamma}_F$	8.98 cm^{-1}
	Asymmetric mode (*ssp*)	$\mathbf{A}_{as}$	-35.00 a.u.
		ω_{as}	2971 cm^{-1}
		$\mathbf{\Gamma}_{as}$	8.65 cm^{-1}
			Value
(Figure 3b)	Offset (*sps*)		4.19 a.u.
	$\chi_{NR}^{(3)}$ (*sps*)		-0.81 a.u.
	Unassigned C-H	$\mathbf{A}$	9.46 a.u.
		ω	2900 cm^{-1}
		$\mathbf{\Gamma}$	8.46 cm^{-1}
	Asymmetric mode (*sps*)	$\mathbf{A}_{as}$	63.46 a.u.
		ω_{as}	2960 cm^{-1}
		$\mathbf{\Gamma}_{as}$	8.62 cm^{-1}

IX. Lipid methyl endgroup orientation analysis using SFG spectroscopy

Using SFG spectroscopy, methyl endgroup orientation could be derived using asymmetric peak ratio measured in different polarization combinations. For methyl group symmetric stretching:[S7]

$$\chi_{xxz,s}^{(2)} = \chi_{yyz,s}^{(2)} = \frac{1}{2} N \beta_{ccc}^{(2)} [(1+a)\langle \cos\theta \rangle - (1-a)\langle \cos^3\theta \rangle] \quad \text{(S20)}$$

$$\chi_{xzx,s}^{(2)} = \chi_{yzy,s}^{(2)} = \chi_{zxx,s}^{(2)} = \chi_{zyy,s}^{(2)} = \frac{1}{2} N \beta_{ccc}^{(2)} (1-a)[\langle \cos\theta \rangle - \langle \cos^3\theta \rangle] \quad \text{(S21)}$$

For the asymmetric stretching:

$$\chi^{(2)}_{yyz,as} = \chi^{(2)}_{xxz,as} = -N\beta^{(2)}_{caa}[\langle\cos\theta\rangle - \langle\cos^3\theta\rangle] \quad \text{(S22)}$$

$$\chi^{(2)}_{zxx,as} = \chi^{(2)}_{zyy,as} = \chi^{(2)}_{yzy,as} = \chi^{(2)}_{xzx,as} = N\beta^{(2)}_{caa}\langle\cos^3\theta\rangle \quad \text{(S23)}$$

Here $a = \beta^{(2)}_{aac} / \beta^{(2)}_{ccc}$. The methyl group orientation can be derived using $\left|\chi^{(2)}_{yyz,as} / \chi^{(2)}_{yzy,as}\right|$. Considering Fresnel coefficients for SFG experiments,[S7] as well as the parameters used in our experiment (input angles of the visible and IR beams are ~60° and 55°, respectively), we have

$$\left|\chi^{(2)}_{ssp,as} / \chi^{(2)}_{sps,as}\right| \approx \left|\chi^{(2)}_{yyz,as} / \chi^{(2)}_{yzy,as}\right| = \left|\frac{\langle\cos\theta\rangle - \langle\cos^3\theta\rangle}{\langle\cos^3\theta\rangle}\right| \quad \text{(S24)}$$

Assuming delta tilt angle distribution of the methyl groups, $\left|\chi^{(2)}_{ssp,as} / \chi^{(2)}_{sps,as}\right| \approx \left|\frac{\cos\theta - \cos^3\theta}{\cos^3\theta}\right|$.

This curve is plotted as Figure 3c in the paper. From the spectral fitting results (Table S3), we have $\left|\chi^{(2)}_{ssp,as} / \chi^{(2)}_{sps,as}\right| \approx 0.55$. This value corresponds to $\theta \approx 35^\circ$.

X. Tilt angle analysis of alkyl chain from OTMS self-assembled monolayer

We used our method to analyze the tilt angle of alkyl chain from an octadecyltrimethoxysilane (OTMS) self-assembled monolayer grown on a silica window substrate. The substrate was first cleaned overnight in a 60°C sulfuric acid bath saturated with potassium dichromate. Then the silica window was rinsed using deionized water multiple times and was further cleaned in an air plasma cleaner. Then it was placed in an OTMS-toluene solution (1 mM) overnight at room temperature for self-assembly. After the self-assembly, the window was taken out and rinsed with toluene multiple times before analysis.

The CARS *spps* spectra from the OTMS bulk and the self-assembled monolayer are shown in Figure S10. The spectra were fit using eq (1) and the results are listed in Table S4. From the bulk spectra we found that $\left|\chi^{(3)}_{spps,s} / \chi^{(3)}_{spps,as}\right| \approx 0.49b^2 \approx 0.58$. Therefore, $b^2 \approx 1.18$, and

$$\left|\chi^{(3)}_{spps,s} / \chi^{(3)}_{spps,as}\right| = b^2 \times \left|\left(0.099\chi^{(3)}_{yxxy,s} + 0.054\chi^{(3)}_{yzzy,s}\right) / \left(0.099\chi^{(3)}_{yxxy,as} + 0.054\chi^{(3)}_{yzzy,as}\right)\right|$$
$$= 1.18 \times \left|\left(0.099\chi^{(3)}_{yxxy,s} + 0.054\chi^{(3)}_{yzzy,s}\right) / \left(0.099\chi^{(3)}_{yxxy,as} + 0.054\chi^{(3)}_{yzzy,as}\right)\right|$$

$\left|\chi^{(3)}_{spps,s} / \chi^{(3)}_{spps,as}\right|$ as a function of θ can be plotted as Figure S11. Here when calculating $\chi^{(3)}_{yxxy}$ or $\chi^{(3)}_{yzzy}$, we need to let $\psi = 0$ (instead of integrating ψ from 0 to 2π) since the alkyl chain of OTMS molecule grown on the silica surface does not have rotation freedom. According to Table S4, $\left|\chi^{(3)}_{spps,s} / \chi^{(3)}_{spps,as}\right| \approx 8.35 / 22.18 \approx 0.38$. This value corresponds to ~35° tilt angle in Figure S11. This result agrees well with the theoretical title angle (35°) of alkyl chains in OTMS when all Si-O bonds are attached to the substrates, as shown in Figure S12.

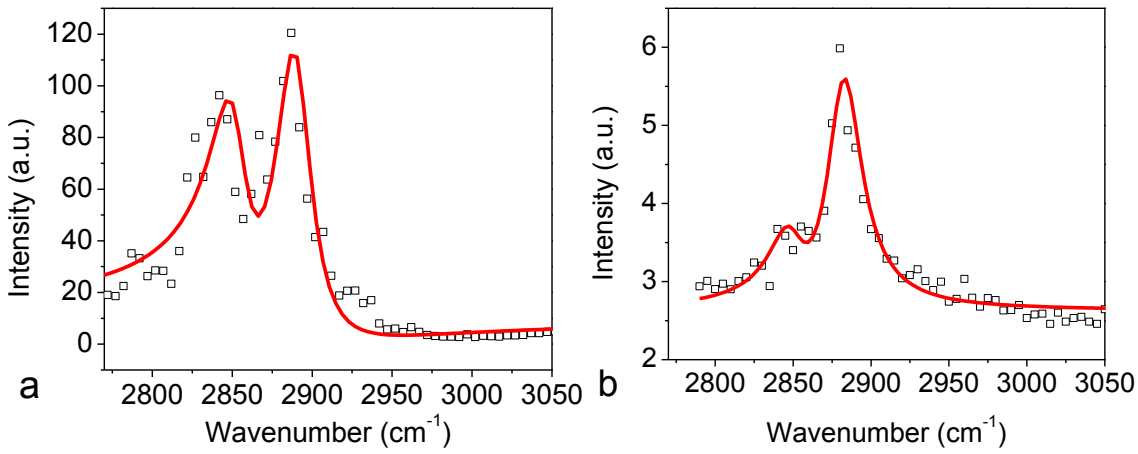

Figure S10. CARS *spps* spectra from (a) the OTMS bulk, and (b) the OTMS self-assembled monolayer on a silica substrate. Dots are experimental data, lines are spectral fitting results.

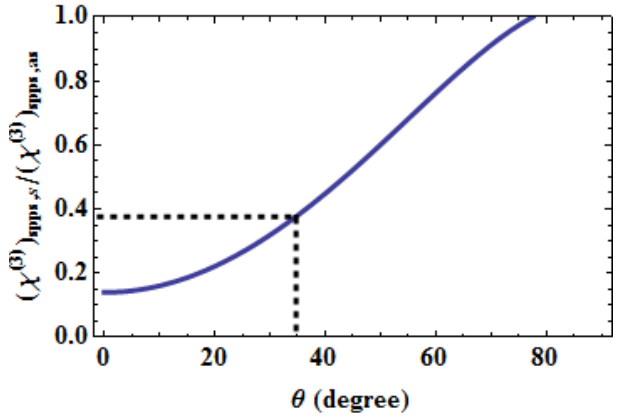

Figure S11. The value of $\left|\chi^{(3)}_{spps,s} / \chi^{(3)}_{spps,as}\right|$ as a function of tilt angle θ when $b^2 \approx 1.18$ and $\psi = 0$.

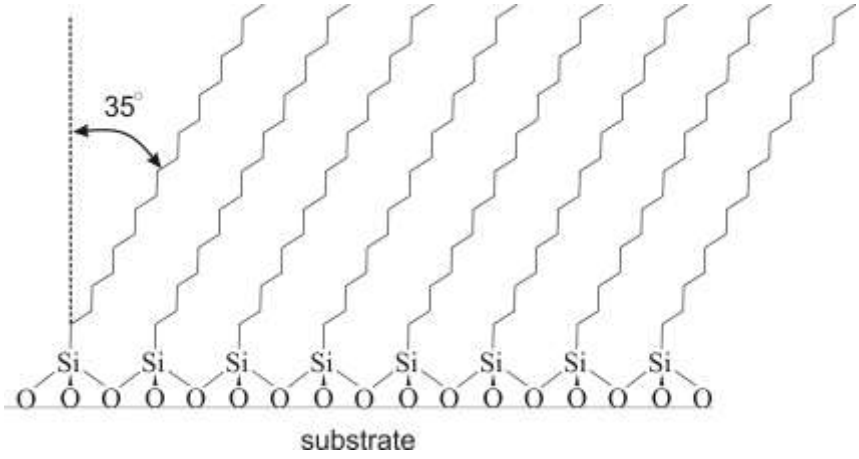

Figure S12. Schematic of an OTMS monolayer grown on a silica window when all Si-O bonds are connected to the substrate. The theoretical tilt angle of the alkyl chain is 35° according to the tetrahedral carbon geometry.

Table S4. CARS spectral fitting results of Figure S10.

	OTMS bulk		Value
(Figure S10a)	Offset (*spps*)		3.20 a.u.
	$\chi^{(3)}_{NR}$ (*spps*)		-2.84 a.u.
	CH_2 symmetric mode (*spps*)	$\mathbf{A}_s$	77.53 a.u.
		ω_s	2853 cm^{-1}
		$\mathbf{\Gamma}_s$	13.70 cm^{-1}
	CH_2 asymmetric mode (*spps*)	$\mathbf{A}_{as}$	133.04 a.u.
		ω_{as}	2880 cm^{-1}

		$\mathbf{\Gamma}_{as}$	13.70 cm^{-1}
	OTMS monolayer		Value
(Figure S10b)	Offset (*spps*)		2.63 a.u.
	$\chi^{(3)}_{NR}$ (*spps*)		-0.01 a.u.
	CH_2 symmetric mode (*spps*)	$\mathbf{A}_s$	8.35 a.u.
		ω_s	2849 cm^{-1}
		$\mathbf{\Gamma}_s$	13.70 cm^{-1}
	CH_2 asymmetric mode (*spps*)	$\mathbf{A}_{as}$	22.18 a.u.
		ω_{as}	2882 cm^{-1}
		$\mathbf{\Gamma}_{as}$	13.70 cm^{-1}

XI. Lipid vesicle CARS signal analysis

Lipid bilayer could be analyzed similarly to the lipid monolayer due to the symmetric arrangement of lipid leaflets. In a CARS microscopic experiment, laser beams are usually combined collinearly, and directed perpendicular to the sample surface. To adopt our method for use for CARS microscopic signal analysis, some modifications are needed. First of all, since transmission geometry is used in the experiment, in eq (S1), (S2), (S3) and (S4) the Fresnel terms can be ignored, because for different polarization conditions they have similar values. We can consider that CARS is simply probing $\chi^{(3)}_{IJKL}$.

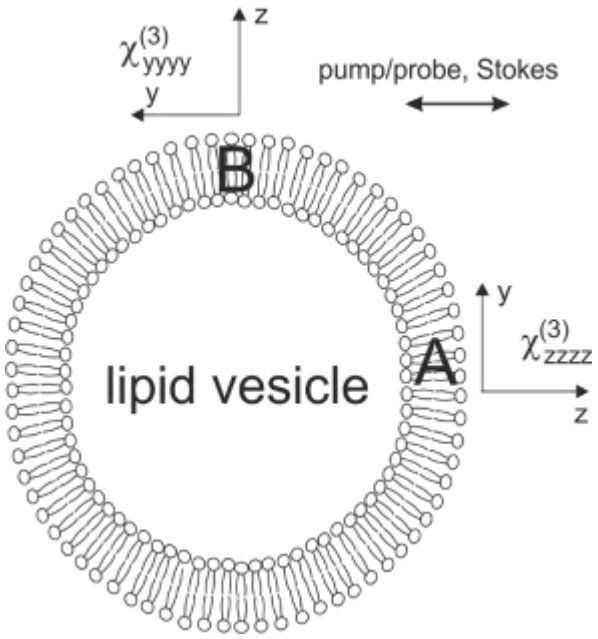

Figure S13. Schematic of a lipid vesicle under a CARS microscopy system and the corresponding coordinate systems chosen at different lipid locations. The double arrow indicates the input laser polarization direction.

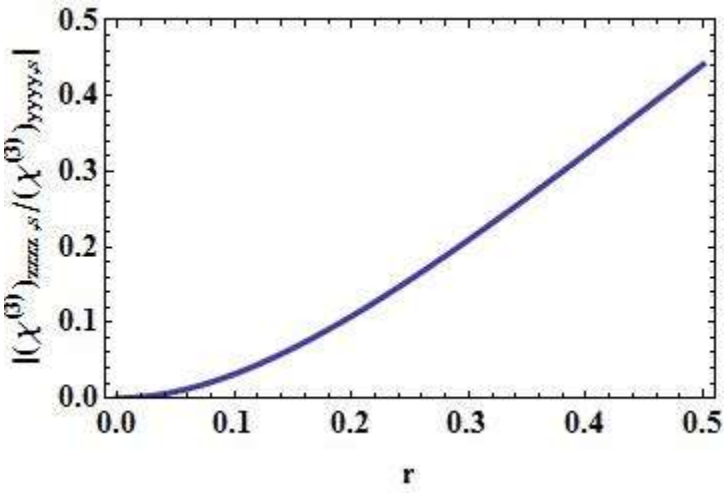

Figure S14. The value of $\left|\chi^{(3)}_{zzzz,s} / \chi^{(3)}_{yyyy,s}\right|$ as a function of r when $\theta = 0$.

Here we assume that the laser focal plane is at the center of the vesicle. z axis is chosen along the surface normal of the local vesicle lipid bilayer. At different locations of a vesicle (as shown in Figure S13), z axis points to different directions. Correspondingly, y axis could be defined as perpendicular to the plane formed by z axis and the laser beam. If the input laser polarization is defined as that shown in Figure S13, at location A CARS microscopic signal measures $\chi^{(3)}_{zzzz}$, while at location B the CARS signal

measures $\chi^{(3)}_{yyyy}$. If we assume lipid alkyl chain has 0° tilt angle with respect to the surface normal *z*, we can set $\theta = 0$ and calculate:

$$\chi^{(3)}_{yyyy}\left(\theta = 0\right) = \frac{C \cdot N}{4\pi^3}\int_0^{2\pi}\int_0^{2\pi} \mathbf{R}_y \boldsymbol{\alpha}'_s \mathbf{R}_y^T \mathbf{R}_y \boldsymbol{\alpha}'_s \mathbf{R}_y^T \mathrm{d}\phi \mathrm{d}\psi$$

$$\chi^{(3)}_{zzzz}\left(\theta = 0\right) = \frac{C \cdot N}{4\pi^3}\int_0^{2\pi}\int_0^{2\pi} \mathbf{R}_z \boldsymbol{\alpha}'_s \mathbf{R}_z^T \mathbf{R}_z \boldsymbol{\alpha}'_s \mathbf{R}_z^T \mathrm{d}\phi \mathrm{d}\psi$$

The value of $\left|\chi^{(3)}_{zzzz,s}\left(\theta = 0\right) / \chi^{(3)}_{yyyy,s}\left(\theta = 0\right)\right|$ is plotted as a function of *r* in Figure S14. We found that this value is *r* dependent and it generally has small values (<0.11when 0<*r*<0.2).

This indicates that CARS CH_2 symmetric stretching signal at location B is usually much stronger than that at location A. Their relative intensity ratio is determined by the value of *r*, which could be obtained using Raman or CARS measurement.[S6] The conclusion we have for the polarization dependent CARS signal of a lipid vesicle is similar yet more quantitative as compared to that obtained from rotation polarization CARS.

REFERENCES:

S1. Zhang, C.; Wang, J.; Khmaladze, A.; Liu, Y.; Ding, B.; Jasensky, J.; Chen, Z., Examining Surface and Bulk Structures Using Combined Nonlinear Vibrational Spectroscopies. *Opt. Lett.* **2011,** *36* (12), 2272-2274.

S2. Tamm, L. K.; McConnell, H. M., Supported Phospholipid Bilayers. *Biophys. J.* **1985,** *47* (1), 105-113.

S3. Zhuang, X.; Miranda, P.; Kim, D.; Shen, Y., Mapping Molecular Orientation and Conformation at Interfaces by Surface Nonlinear Optics. *Phys. Rev. B* **1999,** *59* (19), 12632-12640.

S4. Hirose, C.; Akamatsu, N.; Domen, K., Formulas for the Analysis of Surface Sum-Frequency Generation Spectrum by Ch Stretching Modes of Methyl and Methylene Groups. *J. Chem. Phys.* **1992,** *96* (2), 997-1004.

S5. Wu, H.; Zhang, W.-k.; Gan, W.; Cui, Z.-f.; Wang, H.-f., An Empirical Approach to the Bond Additivity Model in Quantitative Interpretation of Sum Frequency Generation Vibrational Spectra. *J. Chem. Phys.* **2006,** *125*, 133203.
S6. Zhang, C.; Wang, J.; Ding, B.; Jasensky, J., Quantitative Spectral Analysis of Coherent Anti-Stokes Raman Scattering Signal: C-H Stretching Modes of the Methyl Group. *J. Phys. Chem. B* **2014,** *118* (27).
S7. Zhang, C.; Myers, J. N.; Chen, Z., Elucidation of Molecular Structures at Buried Polymer Interfaces and Biological Interfaces Using Sum Frequency Generation Vibrational Spectroscopy. *Soft Matter* **2013,** *9*, 4738-4761.